A Deep Convection Event above the Tunuyán Valley near the Andes Mountains

A. DE LA TORRE

Departmento de Física, Facultad de Ciencias Exactas y Naturales, Universidad de Buenos Aires, Buenos Aires, Argentina

V. DANIEL

Laboratoire de Météorologie Dynamique du CNRS, Ecole Normale Superiéure, Paris, France

R. TAILLEUX

Laboratoire de Météorologie Dynamique du CNRS, Université Pierre et Marie Curie, Paris, France

H. TEITELBAUM

Laboratoire de Météorologie Dynamique du CNRS, Ecole Normale Superiéure, Paris, France

(Manuscript received 4 March 2003, in final form 20 February 2004)

ABSTRACT

Deep convection in the Tunuyán Valley region (33°–34°S, 69°–70°W) on the eastern side of the highest peaks of the Andes Mountains is sometimes associated with damaging hail. Understanding the physical mechanisms responsible for the occurrence of deep convection in that region is therefore a central part of the development of hail suppression projects. In this paper, a case of deep convection that occurred on 22 January 2001 is studied in detail through a combined analysis of radar, satellite, and radiosonde data and numerical simulations using a nonhydrostatic mesoscale atmospheric (Meso-NH) model. The time evolution and stability characteristics are first documented using the data. In order to get insight into the main causes for the deep convection event, numerical simulations of that day were performed. These results are compared with the results corresponding to conditions of 4 January 2001 when no deep convection occurred. The comparison between the 2 days strongly suggests that the deep convection event occurred because of the simultaneous presence of anabatic winds, accumulation of moist enthalpy, and the stability conditions. The present results should be helpful in designing future observational programs in the region.

1. Introduction

The understanding of the generation and development of local winds is of major significance in the description of convection inside a valley. A considerable number of observational results reported before the 1960s (see, e.g., Geiger 1971, and references therein) led to the conclusion that valleys tend to develop their own air circulation, somewhat independently of the ambient wind overflow and with a tendency to flow up or down the valley regardless of the prevailing wind direction. Later observations by means of tethered balloons (Whiteman 1982), Doppler lidar (Post and Neff 1986), and acoustic sounders (Neff and King 1987) confirmed this and brought additional details to the knowledge of internal circulation in different valleys. Geiger (1971) has referred to local winds in the mountains, making a distinction between the ''active'' and ''passive'' influence of the configuration of the land on the air flowing over it. According to this distinction, an active topographic effect takes place wherever differences of temperature and air pressure caused by the land give rise to air currents. Upslope or anabatic winds form during the day when hillside slopes are heated more than the valley floor. Wind speeds up to more than 1 m s^{-1} may be achieved, and it is typically a daytime wind during the summer. After sunrise, anabatic winds have set in, but, since the air in the valley is still colder than the air in the plain outside the valley, the downvalley wind is still blowing. Toward midday, the upvalley wind sets in and feeds the anabatic winds. At this time, this upslope wind is maximum. In the late afternoon, the anabatic winds cease to blow and the upvalley wind continues for a short time. Finally, during the night the cyclic process is reversed and downslope winds set in (katabatic winds). Valley and slope winds then combine to constitute a three-dimensional circulation.

Corresponding author address: A. de la Torre, Departamento de Física, Facultad de Ciencias Exactas y Naturales, Universidad de Buenos Aires, Pabellon I, 1428 Buenos Aires, Argentina.
E-mail: delatorr@df.uba.ar

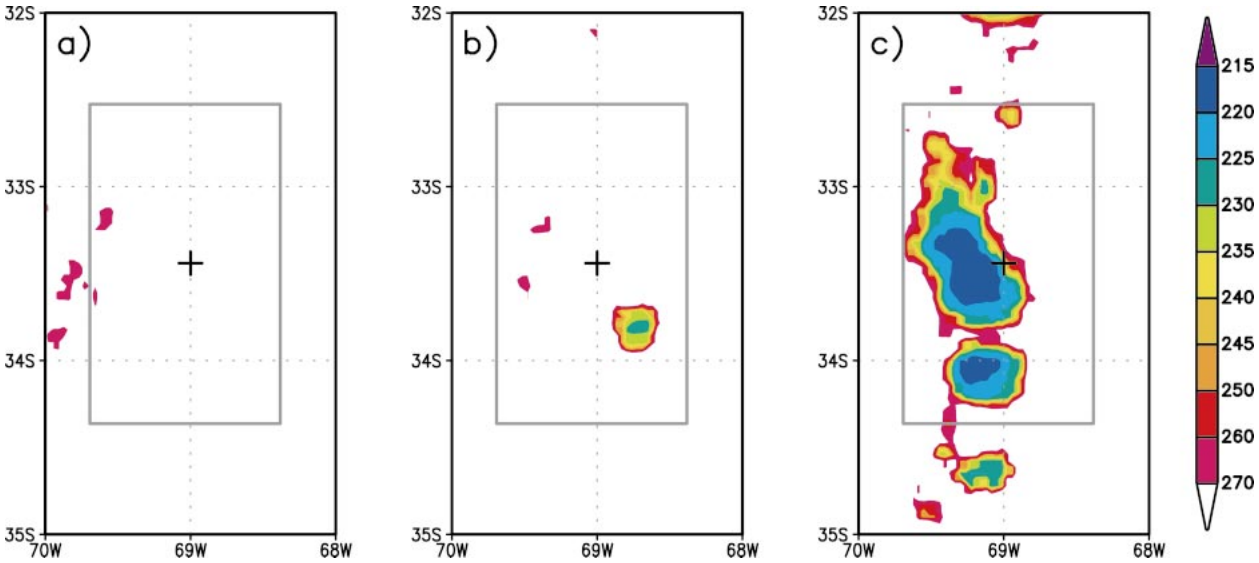

FIG. 1. False color infrared brightness temperature (K) obtained from *GOES-8* on 22 Jan 2001 at (a) 1200, (b) 1500, and (c) 1800 UTC. The box corresponds to the inner geographical domain of the numerical simulation. The location of the radiosonde site is indicated by a cross.

The supposed link between upslope winds and the observed cumuli has been early confirmed from satellite images (Biswas and Jayaweera 1976). Theoretical and numerical works have addressed this problem too. However, only in the last two decades has computing availability made this nonlinear, three-dimensional problem tractable. Mahrer and Pielke (1977) simulated large-scale two-dimensional upslope and downslope winds but without providing details of the slope winds. Egger (1981) examined the flow along a valley. McNider and Pielke (1984) numerically simulated in 3D the secondary flow originating from the difference between the deep pool of cool air in the valley compared to a much shallower surface inversion over the plains into which the valley opens. Banta (1986) numerically modeled in 2D the transient character of upslope flow on the lee side of a heated mountain ridge. He found that the development of the inversion layer is essential for the generation of upslope winds and the stronger ridge-top-level winds produce shorter-lived upslope winds. More recent papers have numerically and experimentally shown the dynamic cycle of slope winds (e.g., Adedodun and Holmgren 1991; Yeh and Chen 1998; Gallee and Pettre 1998; Ramanathan and Srinivasan 1998; Tanaka et al. 2000; Lee and Kimura 2001; Tian and Parker 2002; Parker 2002; Caballero and Lavagnini 2002; Klaic et al. 2002; Lin and Chen 2002).

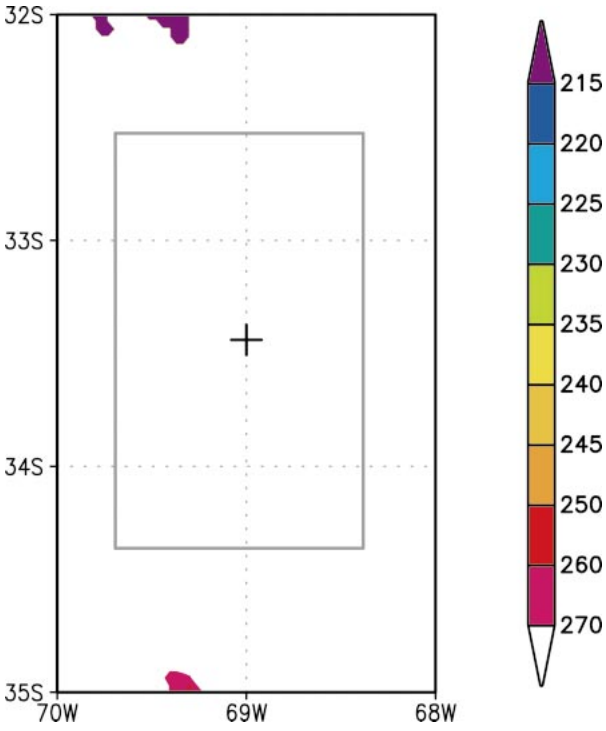

FIG. 2. Same as Fig. 1, but on 4 Jan 2001 at 1800 UTC.

There is a notorious deficiency of observational studies in valley regions in the Southern Hemisphere. East of the Andes range and at middle latitudes, a considerable number of deep valleys mainly aligned in a north–south direction constitute natural laboratories for the study of unusually strong convection events, mainly reported between late spring and early autumn. These processes are sometimes followed by the production of very damaging hail. The purpose of this paper is to present a case study of cumulonimbus formation in the region of Tunuyán Valley (Mendoza, Argentina, 32°–34°S, 69°W), near the highest peaks of the Andes Mountains,

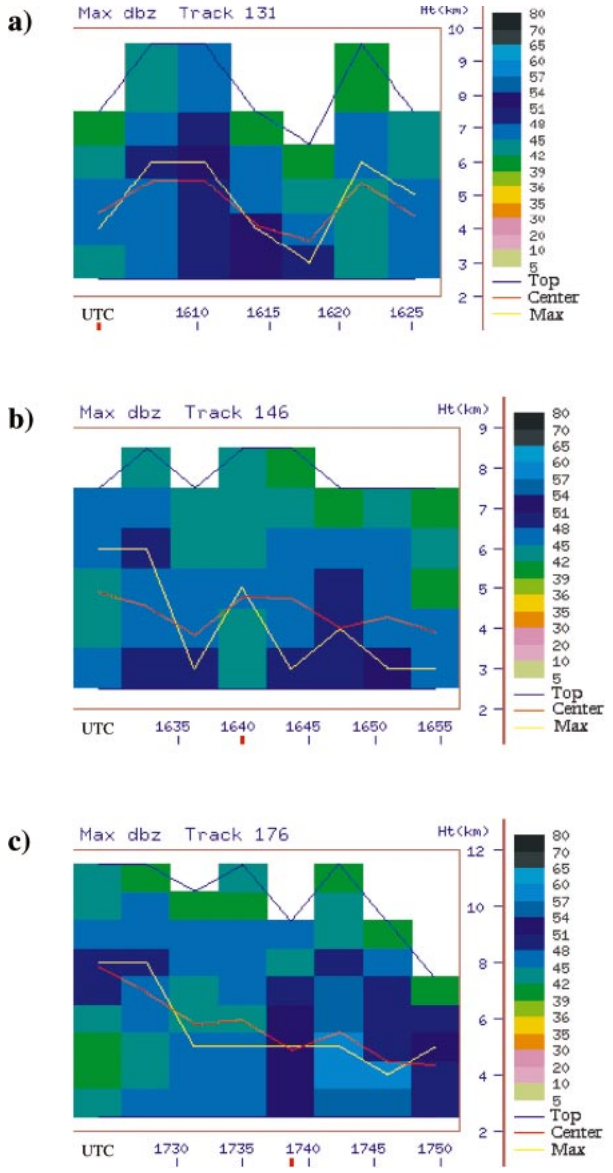

FIG. 3. Reflectivity images (dB*Z*) obtained from the WMI C-band-type radar situated in the Tunuyán Valley. Temporal evolution of cloud top (blue line), center of the cloud (red line), and maximum of reflectivity (yellow line). (a) Beginning at 1601 UTC, (b) beginning at 1628 UTC, and (c) beginning at 1723 UTC.

compared with a case in which no convection occurred. The paper is organized in two parts. First the convective events are described and documented in section 2 using radar and satellite imagery for cloud tops. Section 3 provides a stability analysis of the preconvecting atmosphere using radiosonde data. A modeling effort is developed in section 4 to have access to vertical wind and specific moist enthalpy with mesoscale details better than those we can obtain from European Centre for Medium-Range Weather Forecasts (ECMWF) analysis directly. The results are summarized and discussed in section 5. We show that the triggering of this deep convection event can be explained by the existence of anabatic winds, associated with high convergence of specific moist enthalpy near the ground and favored by instability conditions.

2. Satellite imagery and radar data

The Tunuyán Valley is situated between 33° and 34°S and 69° and 70°W. It mainly runs in a southward direction and is bounded at the west and east by the Andean and Precordillera Mountains, respectively. Its bottom opens and descends northward toward a plain. The highest slope is by far the western one, which rapidly reaches altitudes well above 5 km. The valley is uniformly irrigated by a few Tunuyán River effluents, giving place to the Tunuyán basin.

a. Cloud-top temperature imagery

From infrared images provided by the *Geostationary Operational Environment Satellite-8* (*GOES-8*) and processed by the Servicio Meteorológico Nacional (Argentina), we obtained cloud-top temperatures, which can be estimated with resolution better than 2°. Figures 1a–c show the development of a convection event above the Tunuyán Valley region, on 22 January 2001. At 1200 UTC (hereinafter only UTC reference time is used, solar time = UTC − 4.5 h, approximately), mainly clear-sky conditions are observed over the valley (Fig. 1a). At 1500 (Fig. 1b) one small cloud (situated at 33.8°S, 68.7°W) appeared over the valley. Finally, at 1800 (Fig. 1c) high and thick clouds cover the western slope of the valley following its shape.

Figure 2 displays the temperature retrieved from *GOES-8* but for 4 January at 1800. The valley is free of clouds on this day.

b. Radar observations

The Mendoza region is covered by two Weather Modification, Inc. (WMI), C-band and two MRL5 S-band radars networked for irrigation, electrical and hydrology services, civil defense, and hail suppression operations. In particular, they are used to monitor cloud seeding over the cloud structures. The radar at Tunuyán covers the entire valley with a scanning period of 4 min. The Thunderstorm, Identification, Tracking, Analysis, Nowcasting (TITAN) software package has been added to this radar. The software system ingests radar data and makes it possible to compute a number of storm and track parameters very easily in real time (Mather et al. 1996). In particular, it allows us to identify and follow the evolution of any growing cell of interest and localize its maximum top as a function of time (Figs. 3a–c). In these figures, reflectivities are shown at three illustrative times on 22 January 2001. Each figure displays the evolution of the maximum cloud top, the center of the cloud

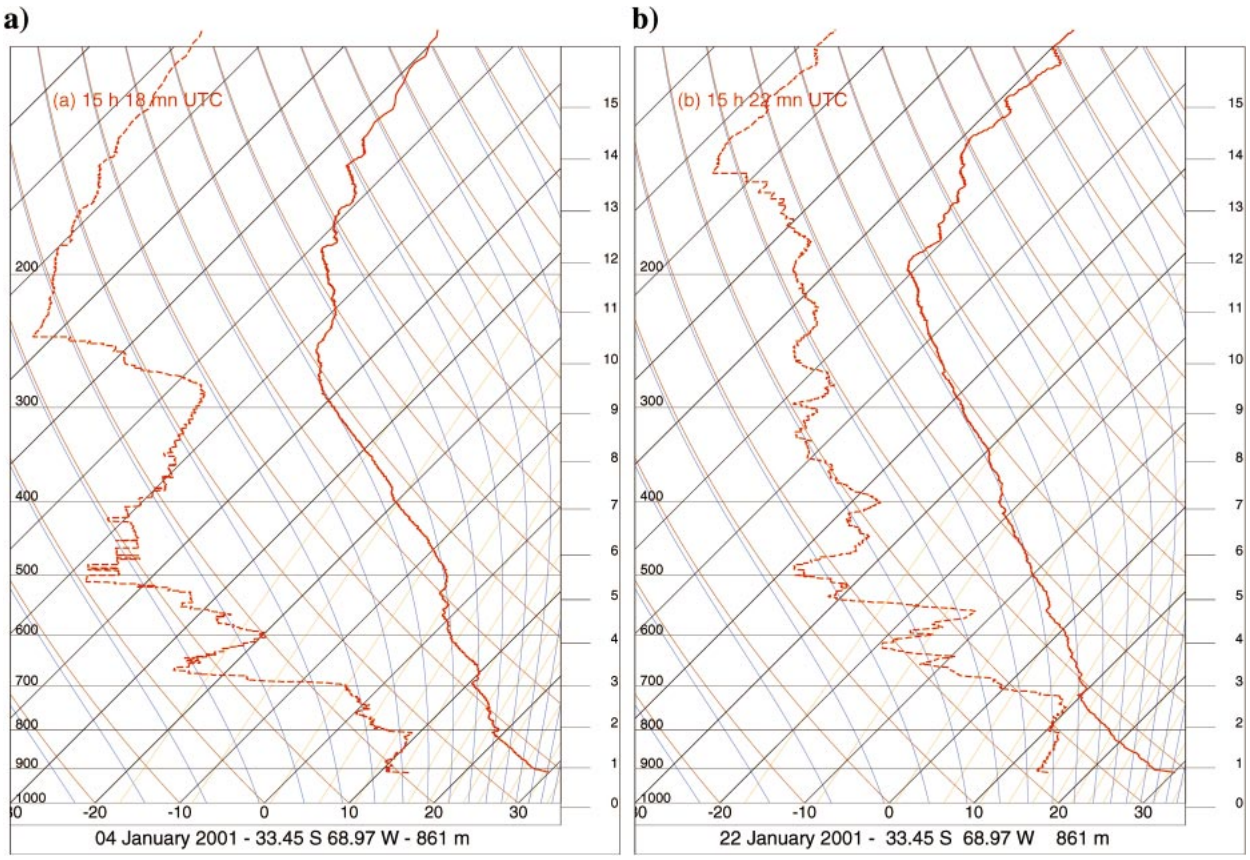

FIG. 4. Skew T_ρ–log$p$ diagram derived from the radiosonde data for (a) 4 Jan 2001 and (b) 22 Jan 2001.

defined as the height of reflectivity centroid, and the altitude of the maximum reflectivity. For our study, we are interested in the cloud-top evolution. At 1602 (Fig. 3a), the radar situated at Tunuyán Valley detects, for the first time, a noticeable reflectivity above the valley region. From 1602 to 1743 (Figs. 3a–c) the reflectivity of the cloud shows tops reaching up to 12 km. The slight oscillating evolution of the cloud tops between 10 and 12 km may be observed. This is probably due to the overshooting of the convective clouds above the neutral buoyancy level. Available data only provide the dry potential temperature from which we can calculate a buoyancy period of 6.5 min; the moist correction is likely to increase this value to better match the observation. The maximum top decreases abruptly after 1743 (around 4 km in less than 10 min).

3. Stability analysis

Regular daily soundings have been performed from a station situated at 33.5°S and 69.0°W between 15 October and 31 March every year from 1999 up to 2001. This was performed in the framework of the hail suppression campaign led by the government of Mendoza. These radiosondes provide raw data of wind, air temperature, pressure, and humidity with high temporal (2 s) and vertical (around 10 m) resolution. They are only tropospheric, for the main motivation is the detection of deep convection events. We look at the results obtained from the radiosonde launched on 22 January 2001 (Fig. 4b) at 1522, during the deep convection event, together with that launched on 4 January (Fig. 4a) at 1518, when convection did not occur. The launching site is not far from the place where we search for these kinds of events, and then the data provide some information regarding the atmospheric conditions in the region. Figure 4b is a skew T_ρ–log$p$ diagram derived from the radiosonde launched on 22 January. In the simplest case, a parcel lifted from the boundary layer will usually be first negatively buoyant up to its level of free convection (LFC) and then become positively buoyant up to the level of neutral buoyancy (LNB). In the literature convective inhibition (CIN) is conventionally defined as the work of buoyancy forces over the pressure range where the parcel is negatively buoyant, and CAPE as the work of buoyancy forces over the region where it is positively buoyant (Emanuel 1994; Parker 2002). In the present sounding we find that the buoyancy of a parcel lifted from some arbitrary level P_i can be alternatively negatively and positively buoyant

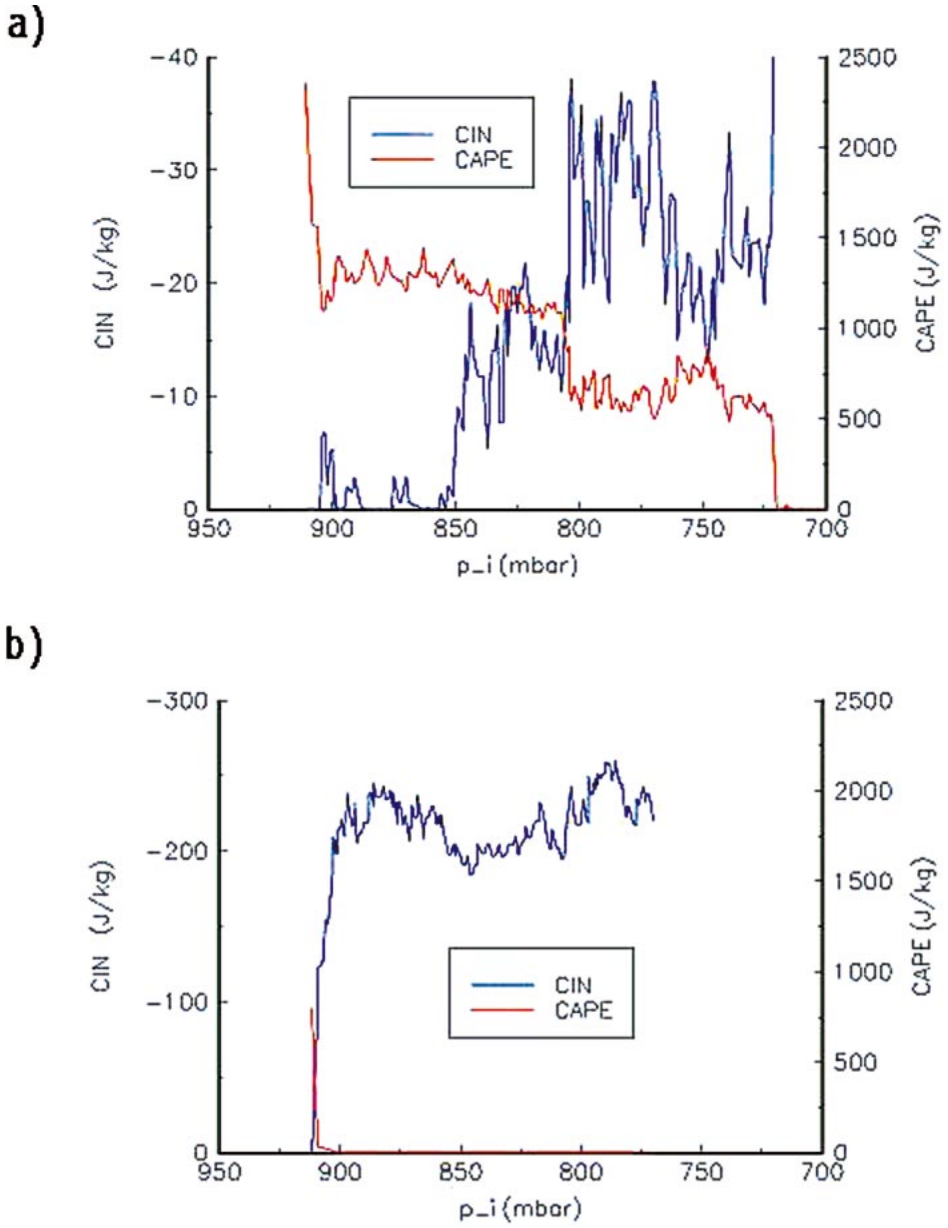

FIG. 5. CIN (blue line) and CAPE (red line) as a function of pressure, as deduced from the radiosonde launched on (a) 22 Jan 2001 and (b) 4 Jan 2001.

several times before reaching the ''true'' LFC, making it difficult to use the conventional definition of CIN. For this reason, we compute the function $W(p_i, p)$, which represents the work of buoyancy forces of a parcel lifted from the pressure p_i up to the level p, and take as our definition CIN $(p_i) = \min[W(p_i, p)]$, for p between p_i and $p_{\max}$, where $p_{\max}$ is taken below LNB. In the same way, we take for the definition of CAPE(p_i) $= \max[W(p_i, p)]$, for p taken between p_i and the top of the sounding, which is somewhat different from the conventional definition, as it includes the work of buoyancy forces from the level p_i, whereas conventional definitions usually start the integration from LFC and thus consider only the work done by the positive buoyant parcels.

The advantage of the present definition is to provide an easy way to compute CIN(p_i) and CAPE (p_i) from $W(p_i, p)$, even when the soundings are very complex, that is, associated with several local extrema in the function $W(p_i, p)$. Another interest of the present approach is to provide insight into the amount of air susceptible to feed the deep convective updrafts, an issue that was recently evoked at a deep convection workshop in Washington, D.C. (Tao et al. 2003) and is likely to receive

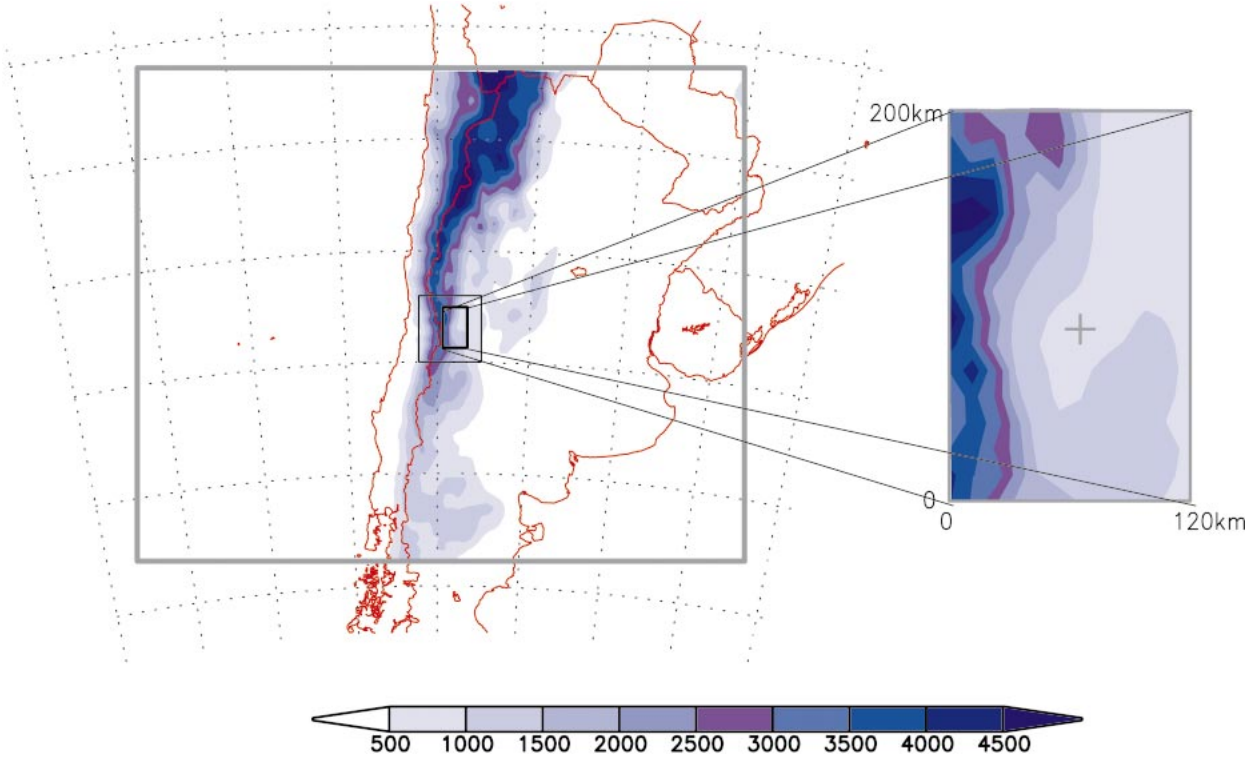

FIG. 6. (left) Geographical domain used for the nested simulation. The outer frame shows the 30-km grid mesh domain and its topography (m); the location of the 10-km (3 km) grid mesh domain is indicated with thin (thick) black lines. (right) Topography (m) of the 3-km grid mesh domain and location (cross) of the radiosonde site.

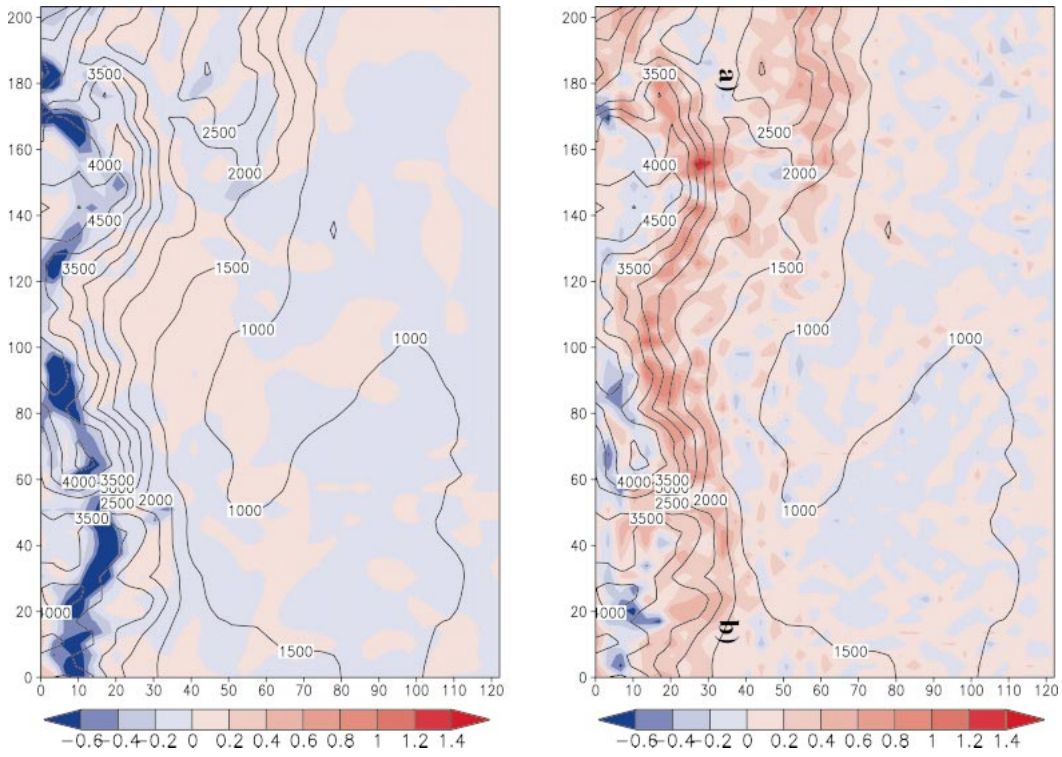

FIG. 7. Vertical velocity (m s^{-1}) calculated from the Meso-NH model at 200 m AGL on 22 Jan 2001 at (a) 1000 and (b) 1600 UTC.

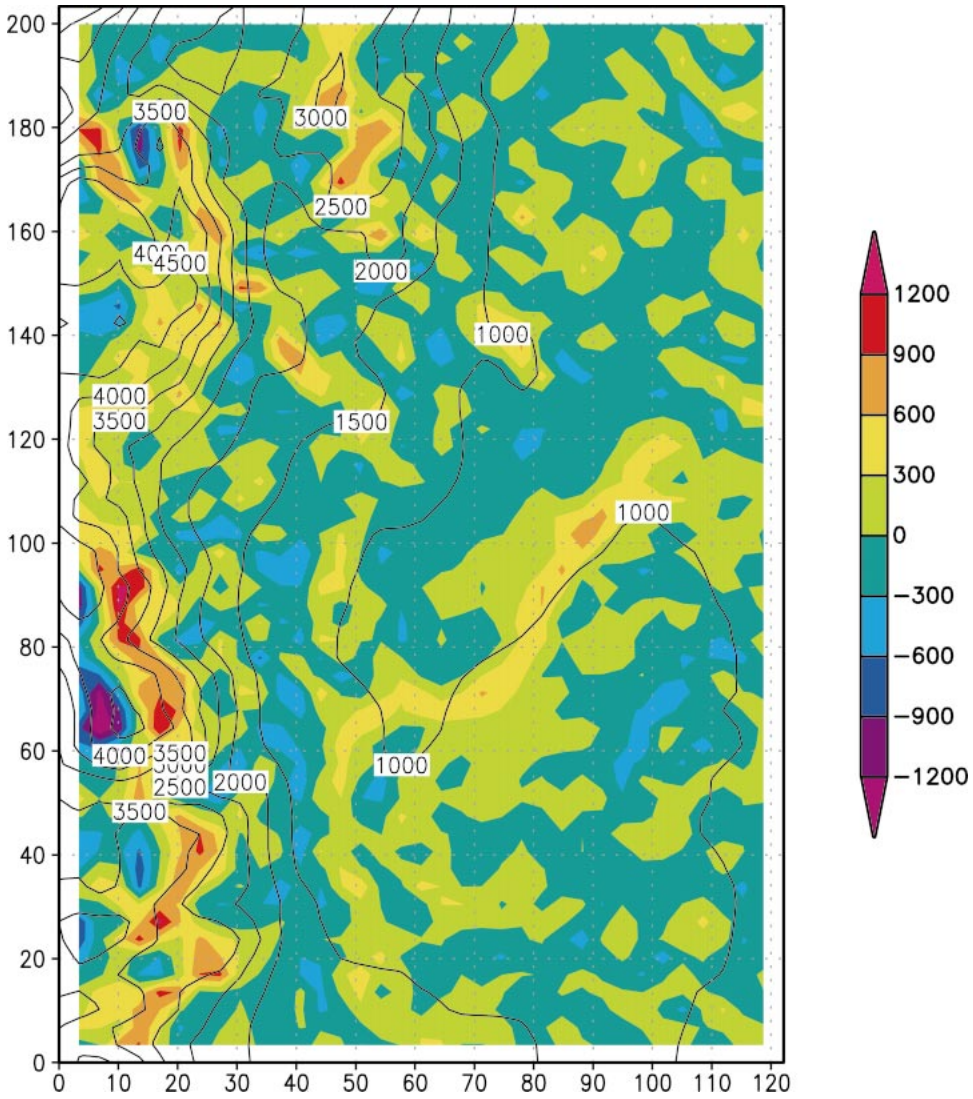

FIG. 8. Specific moist enthalpy convergence (W kg^{-1}) calculated from the Meso-NH model at 1600 UTC and 200 m AGL.

increased attention in the near future. In the present case (Fig. 5a), the sounding is characterized by four distinct layers of air: 1) A very thin superficial layer of about 10 mb that is absolutely unstable, with high values of CAPE (>2000 J kg^{-1}); 2) the layer up to 850 mb is characterized by the presence of a significant and relatively constant CAPE of 1200–1300 J kg^{-1}, with layers of moderate CIN (of the order of 2 to 5 J kg^{-1}) alternating with layers that are absolutely unstable, and thus free to convect; 3) the layer between 850 and 725 mb is characterized by a very high value of CIN (>10 J kg^{-1}) and a much lower value of CAPE (1000 to 600 or 700 J kg^{-1}); 4) the air about 725 mb has no CAPE and is absolutely stable to any finite-amplitude displacements.

In conclusion, the air in the region between the surface and 850 mb most likely forms the convective updrafts of the early stages of a convective event. The overlying air (between 850 and 750 mb), despite large values of CIN, may also feed the convective updrafts in the presence of anabatic winds, since they are conditionally unstable. Incidentally, we observe in Fig. 4b that the LNB is found at 12 km, and the temperature at this level is close to the cloud-top temperature seen in Fig. 1c (around −60°C). As shown above, this altitude almost coincides with that given by radar data.

On 4 January (Figs. 4a and 5b), we can see that the atmosphere appears much more stable on this day. This is due to (i) much dryer conditions, especially in the boundary layer and in the free troposphere, resulting in a condensation level about 50 mb higher, which makes it more difficult for clouds to form, (ii) more significant CIN values, and (iii) a relatively weaker value of CAPE, implying a weaker conditional instability.

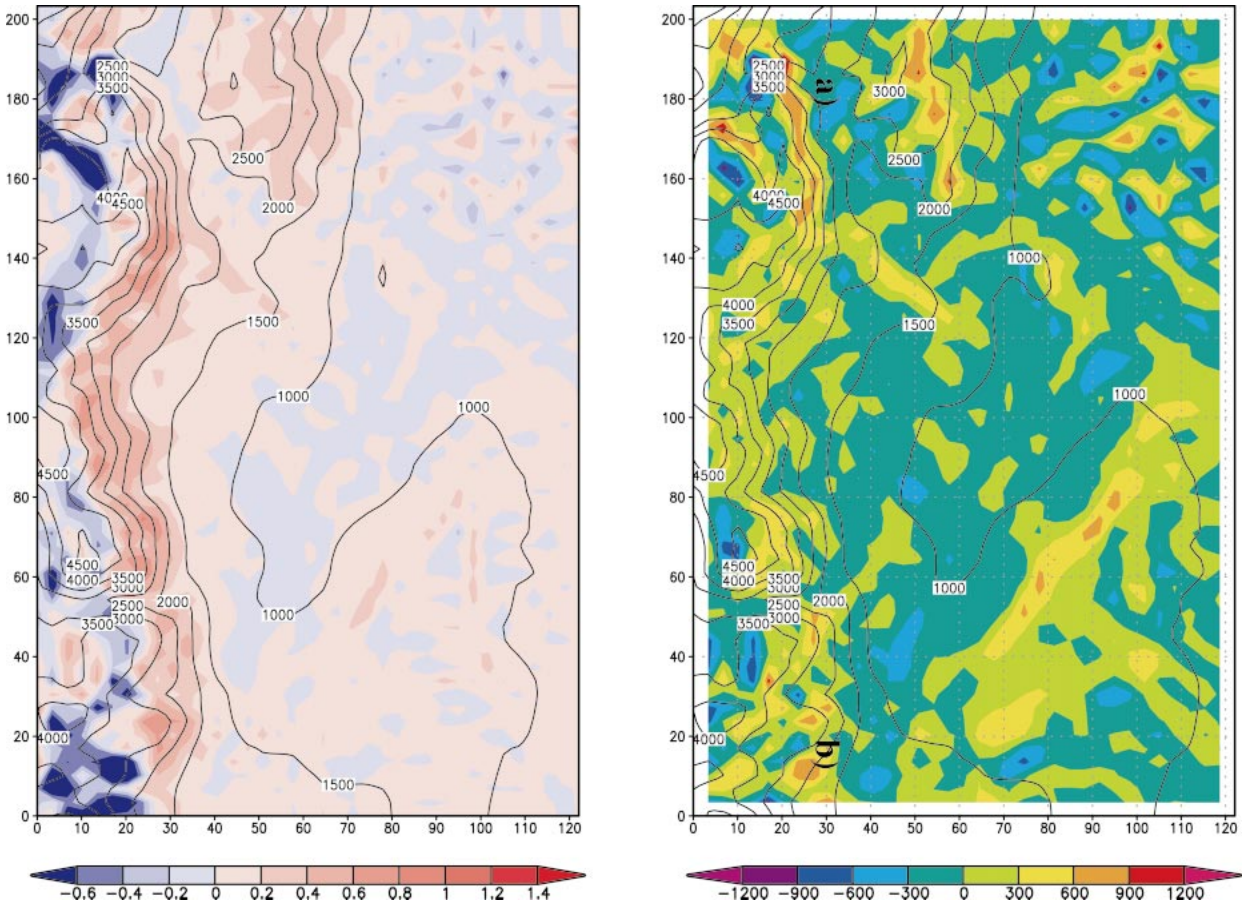

FIG. 9. (a) Vertical velocity (m s^{-1}) and (b) specific moist enthalpy convergence (W kg^{-1}) calculated from the Meso-NH model on 4 Jan 2001 at 1600 UTC.

4. Mesoscale atmosphere conditions obtained from the Meso-NH model

The Meso-NH atmospheric simulation system is a nonhydrostatic mesoscale atmospheric model based on an advanced set of anelastic equations (Lafore et al. 1998). It allows the simultaneous simulation of various scales of motion, by the so-called interactive grid-nesting technique. Richard et al. (2003) have developed this model to study convection phenomena. Initial conditions and boundary conditions of the outermost model are obtained by interpolating the ECMWF operational analyses available every 6 h. These analyses are performed after the assimilation of a great amount of atmospheric data. A nonhydrostatic model allows us to have access to the vertical wind and specific moist enthalpy convergence (SMEC) with resolution enough to understand their role in the generation of convection in the valley.

Figure 6 (left) shows three concentric boxes. The spatial resolution in the outer, middle, and inner box is 30, 10, and 3 km, respectively. The inner box is seen amplified at the right. In this box, the cross shows the center of the valley, from which radiosondes are regularly launched. (see below). False colors simulate the relief (in meters). Let us see now in Fig. 7 the results calculated for the vertical velocity at 200 m above ground level, at 1000 (Fig. 7a) and 1600 (Fig. 7b). As expected, at 1000 the vertical wind is negative over the west side of the valley, while at 1600 it becomes positive, with a maximum value of 1 m s^{-1}. This positive wind velocity, which appears when the west slope of the valley has been heated by the sun, is typically an anabatic wind. A quantitative knowledge previous to local moist convection events is provided by the SMEC, $-\mathrm{div}(\mathbf{u}k)$, where $\mathbf{u}$ is the horizontal velocity and k the specific moist enthalpy (see, e.g., Emanuel 1994):

$$k = (c_{\mathrm{pd}} + r_t c_l)T + L_v r. \quad (1)$$

Here, c_{pd}, c_l, r_t, r, and L_v are the heat capacity of dry air at constant pressure and of liquid water, the total water content (except ice) per unit mass of dry air, the mixing ratio, and the latent heat for the transition liquid vapor, respectively. At constant pressure this is a conserved quantity, regardless of whether the transformation is reversible or not, and if no heat is added other than latent heat associated with the phase changes.

SMEC has also been calculated from the Meso-NH model, and Fig. 8 shows the results obtained at 1600 and 200 m above ground level. High positive SMEC values at the western slope of Tunuyán Valley are coincident in place and shape with cloud tops (Figs. 1 and 3) and anabatic wind (Fig. 7). Figure 9a displays the vertical wind on 4 January at 1600 UTC. Anabatic wind is also present on the western slope of the valley. This is not the case for the SMEC values (Fig. 9b), which appear much smaller than those of 22 January. The results of this section together with the stability analysis show that anabatic wind is not enough to generate convection in the valley. Other conditions such as large SMEC and instability are necessary.

5. Conclusions

We have studied a deep convection event above the Tunuyán Valley region, immediately east of the highest peaks of the Andes Mountains. This case has been compared to a day without convection. Both cases were documented using cloud-top imagery derived from *GOES-8.* The time evolution of the convection has been followed using radar data. The description was completed by stability analysis using radiosondes. This analysis revealed important differences between the two cases under consideration. The atmosphere is much more stable on the day without convection that in the convective case. To derive vertical wind and specific moist enthalpy convergence with better precision than from ECMWF analysis we used the Meso-NH mesoscale model. As expected, anabatic winds are present on both days, but specific moist enthalpy convergence is 3 times higher on the convective day. A preliminary conclusion of this study is that even if anabatic winds play an important role in the development of convective events in the valley, they are not sufficient enough to achieve the phenomena. Specific moist enthalpy convergence near the ground and instability conditions seems to be necessary. A number of cases with and without convection are under study to determine more precisely the local and regional atmospheric conditions able to generate convection in this valley.

Acknowledgments. We are grateful to the Consejo Nacional de Investigaciones Cientificas y Técnicas (Argentina) and the Centre Nationale de la Recherche Scientifique (France) for providing the necessary funding to allow the meeting of the authors. We also thank to the European Centre for Medium-Range Weather Forecasts for the use of the analyses. Servicio Meteorólogico Nacional (Argentina) provided the *GOES-8* imagery data. We wish to thank Dr. H. Martinez and to the government of Mendoza, Argentina, for delivering the radiosonde data as well as the radar imagery.

REFERENCES

Adedodun, J. A., and B. Holmgren, 1991: Acoustic sounder detection of anabatic/katabatic winds in Abisko, N. Sweden. *Renewable Energy,* **1,** 77–89.

Banta, R. M., 1986: Daytime boundary layer evolution over mountainous terrain. Part II: Numerical studies of upslope flow duration. *Mon. Wea. Rev.,* **114,** 1112–1130.

Biswas, A. K., and W. Jayaweera, 1976: NOAA-3 satellite observations of thunderstorms in Alaska. *Mon. Wea. Rev.,* **104,** 292–297.

Caballero, R., and A. Lavagnini, 2002: A numerical investigation of the sea breeze and slope flows around Rome. *Nuovo Cimento,* **25C,** 287–304.

Egger, J., 1981: Thermally forced circulations in a valley. *Geophys. Astrophys. Dyn.,* **130,** 255–279.

Emanuel, K. A., 1994: *Atmospheric Convection.* Oxford University Press, 580 pp.

Gallee, H., and P. Pettre, 1998: Dynamical constraints on katabatic wind cessation in Adelie Land, Antartica. *J. Atmos. Sci.,* **55,** 1755–1770.

Geiger, R., 1971: *The Climate near the Ground.* Harvard University Press, 611 pp.

Klaic, Z. B., T. Nittis, I. Kos, and N. Moussiopoulos, 2002: Modification of the local winds due to hypothetical urbanization of the Zagreb surroundings. *Meteor. Atmos. Phys.,* **79,** 1–12.

Lafore, J. P., and Coauthors, 1998: The Meso-NH atmospheric simulation system. Part I: Adiabatic formulation and control simulations. *Ann. Geophys.,* **16,** 90–10.

Lee, S. H., and F. Kimura, 2001: Comparative studies in the local circulations induced by land-use and by topography. *Bound.-Layer Meteor.,* **101,** 157–182.

Lin, C. Y., and C. S. Chen, 2002: A study of orographic effects on mountain-generated precipitation systems under weak synoptic forcing. *Meteor. Atmos. Phys.,* **81,** 1–25.

Mahrer, Y., and R. A. Pielke, 1977: The effects of topography on land and sea breezes in a two-dimensional mesoscale model. *Mon. Wea. Rev.,* **105,** 1152–1162.

Mather, G. K., M. J. Dixon, and J. M. deJager, 1996: Assessing the potential for rain augmentation—The Nelspruit randomized convective cloud seeding experiment. *J. Appl. Meteor.,* **35,** 1465–1482.

McNider, R. T., and R. A. Pielke, 1984: Numerical simulation of slope and mountain flows. *J. Climate Appl. Meteor.,* **23,** 1441–1453.

Neff, W. D., and C. W. King, 1987: Observations of complex-terrain flows using acoustic sounders: Experiments, topography and winds. *Bound.-Layer Meteor.,* **40,** 363–392.

Parker, D. J., 2002: The response of CAPE and CIN to tropospheric thermal variations. *Quart. J. Roy. Meteor. Soc.,* **128,** 119–130.

Post, M. J., and W. D. Neff, 1986: Doppler lidar measurements of winds in a narrow mountain valley. *Bull. Amer. Meteor. Soc.,* **67,** 274–281.

Ramanathan, N., and K. Srinivasan, 1998: Simulation of airflow in Kashmir Valley for a summer day. *J. Appl. Meteor.,* **37,** 497–508.

Richard, E., S. Cosma, P. Tabary, J.-P. Pinty, and M. Hagen, 2003: High-resolution numerical simulations of the convective system observed in the Lago Maggiore area on 17 September 1999 (MAP IOP2a). *Quart. J. Roy. Meteor. Soc.,* **129,** 543–563.

Tanaka, H. L., D. Nohara, and M. Yokoi, 2000: Numerical simulation of wind hole circulation and summertime ice formation at Ice Valley in Korea and Nakayama in Fukushima, Japan. *J. Meteor. Soc. Japan,* **78,** 611–630.

Tian, W. S., and D. J. Parker, 2002: Two-dimensional simulation of orographic effects on mesoscale boundary-layer convection. *Quart. J. Roy. Meteor. Soc.,* **128,** 1929–1952.

Whiteman, C. D., 1982: Breakup of temperature inversions in deep mountain valleys: Part I. Observations. *J. Appl. Meteor.,* **21,** 270–289.

Yeh, H. C., and Y. L. Chen, 1998: Characteristics of rainfall distributions over Taiwan during the Taiwan Area Mesoscale Experiment (TAMEX) *J. Appl. Meteor.,* **37,** 1457–1469.